IEEE Photonics Journal
An IEEE Photonics Society Publication

High-Resolution Distributed Dispersion Characterization for Polarization Maintaining Fibers Based on a Closed-Loop Measurement Framework

Volume 9, Number 3, June 2017

Zhangjun Yu
Jun Yang
Yonggui Yuan
Feng Peng
Hanyang Li
Changbo Hou
Chengcheng Hou
Zhihai Liu
Libo Yuan

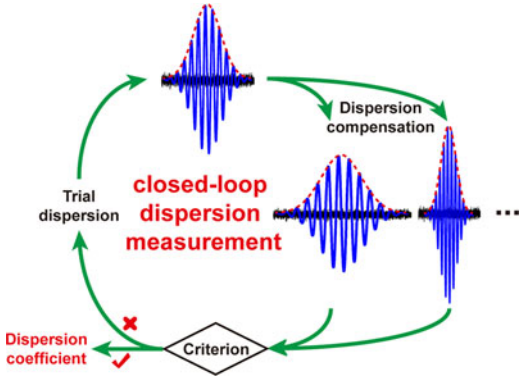

DOI: 10.1109/JPHOT.2017.2702567
1943-0655 © 2017 IEEE

High-Resolution Distributed Dispersion Characterization for Polarization Maintaining Fibers Based on a Closed-Loop Measurement Framework

Zhangjun Yu,[1,2] Jun Yang,[1,2] Yonggui Yuan,[1,3] Feng Peng,[1,2] Hanyang Li,[1,2] Changbo Hou,[1,3] Chengcheng Hou,[1,2] Zhihai Liu,[1,2] and Libo Yuan[1,2]

[1]Key Lab of In-fiber Integrated Optics, Ministry Education of China, Harbin Engineering University, Harbin 150001, China
[2]College of Science, Harbin Engineering University, Harbin 150001, China
[3]College of Information and Communications Engineering, Harbin Engineering University, Harbin 150001, China

DOI:10.1109/JPHOT.2017.2702567

Manuscript received April 5, 2017; revised May 5, 2017; accepted May 5, 2017. Date of publication May 10, 2017; date of current version May 19, 2017. This work was supported by the National Natural Science Foundation of China under Grant 61422505, Grant 61635007, Grant 61307104, and Grant 61405044; in part by the Program for New Century Excellent Talents in University (NCET-12-0623); in part by the National Key Scientific Instrument and Equipment Development Project (No. 2013YQ040815); and in part by the Harbin Science and Technology Innovative Talents Project of Special Fund (2015RAYXJ009).
Corresponding author: J. Yang (e-mail: yangjun@hrbeu.edu.cn).

Abstract: A closed-loop dispersion measurement framework (CLDM) is proposed. Carrying out dispersion compensation with an arbitrary trial dispersion on the interferogram under test, and using a criterion function as feedback to adjust the trial dispersion until the optimum is reached the trial dispersion is the measured result. The CLDM framework is not only noise-robust but can also cope with the case of multiple peaks that provides high resolution. We use it to measure the distributed birefringence dispersion (BD) chromatic dispersion difference of the two polarized modes of polarization maintaining fibers (PMFs). In this regime, the optimum of dispersion compensation is that the signal energy of every peak in the interferogram is concentrated. Thus, we present a criterion function to evaluate the signal energy concentration. Theoretical and experimental demonstration of this method is implemented. In addition, the spatial resolution ($<$10 cm) is discussed. Eventually, a $\approx$ 3 km-length PMF coil is tested. The measurement error for BD and its slope @1550 nm are $< 5 \times 10^{-4}$ ps/nm/km and 2×10^{-4} ps/nm^2/km, respectively.

Index Terms: Fiber characterization, polarization-maintaining fibers, fiber optics sensors.

1. Introduction

Polarization maintaining fiber (PMF) has been widely used within the field of fiber-optic communication [1] and sensing [2]. It is well known that the chromatic dispersion (CD) of PMFs is a significant nature in fiber-optic communication. However, in fiber-optic sensing, we care more about the CD difference of the two polarized modes of PMFs [3], which is known as birefringence dispersion (BD) [4]. BD degrades the spatial resolution when a PMF is used for distributed sensing [5]. Fortunately, dispersion compensation (DC), or elimination, can be implemented if the distributed BD of a PMF is measured.

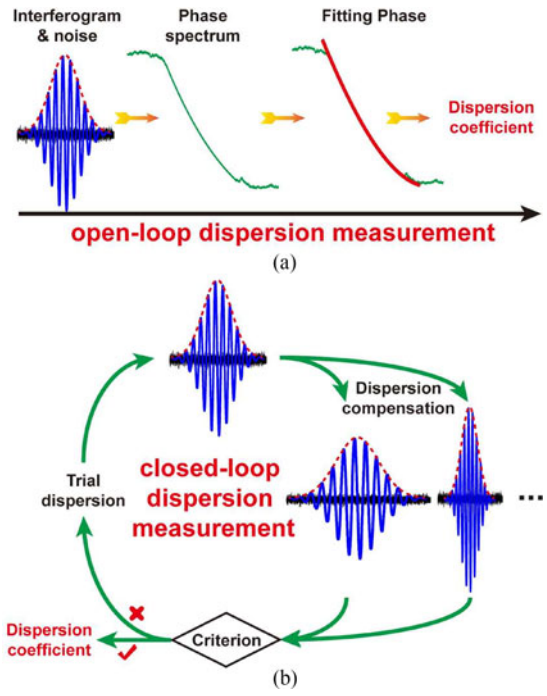

Fig. 1. (a) Open-loop and (b) closed-loop measurement procedures for birefringence/chromatic dispersion.

Because of the definition, the BD of a PMF could be measured with those methods for accurately characterizing the CD, such as the time domain (TD) [6] or spectral domain (SD) [7], [8] white light interferometry (WLI). These methods could also directly measure the BD if we regard the PMF as a Mach-Zehnder interferometer [4], [9], [10]. In the case of TD-WLI, the interferogram with noise will be taken the Fourier transform to obtain its phase spectrum as shown in Fig. 1(a). Subsequently, the phase spectrum contaminated by noise will be taken polynomial fitting, then the fitting coefficients are the dispersion coefficient we want to measure [9]. An alternative method is taking Gaussian fitting on the envelope of the interferogram, and the dispersion is determined by the envelope broadening factor [11]. The unbalanced SD-WLI [12] is familiar with the former. The difference is that the phase spectrum is obtained from the channel spectrum captured by an optical spectrum analyzer. The balanced SD-WLI [10] is directly taking non-linear curve fitting on the channel spectrum to obtain the balanced-wavelength for a given group delay (GD), which requires multi-measurements in order to obtain the wavelength-GD curve. We refer to these sequential measurement methods above as open-loop dispersion measurement methods, which are vulnerable to noise. To this end, we presented a method to improve the noise robustness of TD-WLI using the weighted least square fitting [13]. However, the performance of this method is extremely limited by the signal to noise ratio (SNR) as well.

In this paper, we present a closed-loop dispersion measurement method using the signal energy concentration as feedback. It is demonstrated that it could simultaneously measure the 2nd order BD, the third-order BD, and even higher-order BD in the case of multiple peaks. Experimental results show that the measurement accuracy is very high even if the peaks submerge in the noise. It is evident that this method is also suitable for CD measurement.

2. Theory

Fig. 2(a) shows the setup for distributed polarization crosstalk measurement based on time-domain white light interferometry. Broadband light with FWHM of 50 nm and centered at

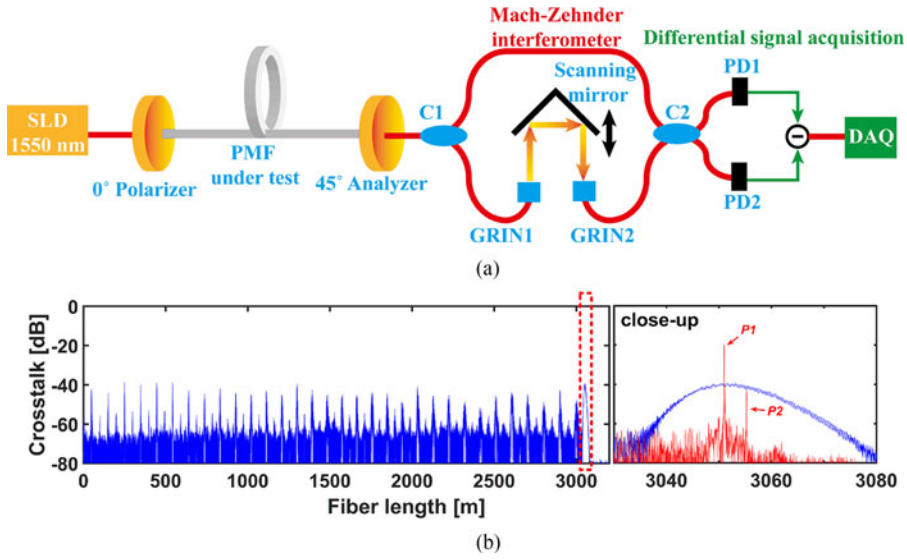

Fig. 2. (a) Measurement setup based on TD-WLI. SLD: superluminescent diode at 1550 nm with FWHM of 50 nm; C1, C2: coupler; GRIN1, GRIN2: GRIN lens; PD1, PD2: photodiodes; DAQ: data acquisition. (b) Distributed polarization crosstalk for a 3051 m-length PMF coil (≈13 cm in diameter).

1550 nm is injected into a 0° polarizer. After transmitting through the PMF under test, the light output to a 45° analyzer. Both the excited light and the coupled light are injected into a Mach-Zehnder interferometer with the same proportion. In the end, a differential signal acquisition system is used to obtain the interferogram. The length of PMF is ≈3 km, and the coil diameter is ≈15 cm. The interferogram, $I_0(x)$, output from the TD-WLI-based setup in Fig. 2(a) is shown in Fig. 2(b). It is generated by the interference between the TM and TE modes of the PMF under test. There is one-to-one correspondence between the position of the scanning mirror, d, and the coordinate x in the interferogram function. Furthermore, the relationship between the moved distance of the scanning mirror, Δd, and the increment of the coordinate x, Δx, could be expressed as $\Delta x = \Delta d/2$. Nevertheless, when the optical path of the scanning arm of the Mach-Zehnder interferometer reaches the minimum, i.e. $d = 0$, the coordinate x is probably not equal to zero, which also depends on the optical path of the other interferometer arm (the so-called reference arm). To characterize the fiber coil with large length, we should adjust the optical path difference between the scanning arm and the reference arm until the optical path of the scanning arm (when $d = 0$) is slightly larger than the optical path of the reference arm. The complex representation of $I_0(x)$ can be expressed as [14]

$$H_0(x) = -\mathrm{i}\int_0^L \Gamma_0(\eta)\int_0^{+\infty} G(\sigma)e^{\mathrm{j}[2\pi\sigma x+\Delta\beta(\sigma)(L-\eta)]}\mathrm{d}\sigma\mathrm{d}\eta \tag{1}$$

where $\Gamma_0(\eta)$ is the mode coupling coefficient (MCC) between TM and TE modes of the L-length PMF at distance η from the output end; $G(\sigma)$ is the power spectrum of light source at wavenumber σ; and $\Delta\beta(\sigma)$ is the propagation constant difference of the two modes. The non-linear phase term is $\varphi_{\mathrm{non}} = \Delta\beta_{\mathrm{non}}(L-\eta)$, where $\Delta\beta_{\mathrm{non}}$ is the non-linear term of $\Delta\beta(\sigma)$. Taking the Taylor-expansion of the nonlinear phase term $\varphi_{\mathrm{non}}(\sigma)$ with respect to the wavenumber σ, we obtain $\varphi_{\mathrm{non}}(\sigma) = SBD\cdot(\sigma-\sigma_0)^2/2 + TBD\cdot(\sigma-\sigma_0)^3/6+\cdots$, where σ_0 is the wavenumber corresponding to the central wavelength, SBD and TBD are second- and third-order BD, respectively

The dispersion compensation operation shown in Fig. 1(b) can be expressed as

$$I(x) = \mathcal{F}^{-1}\left\{\mathcal{F}[I_0(x)]e^{-\mathrm{i}\varphi_{\mathrm{non,trial}}(\sigma)}\right\} \tag{2}$$

where $\varphi_{\mathrm{non,trial}}(\sigma)$ is the phase term containing the information of trial dispersion; $\mathcal{F}$ and $\mathcal{F}^{-1}$ are Fourier transform and inverse Fourier transform operator, respectively. The BD will spread the

signal energy in time domain. For instance, the second-order BD will broaden the envelope of the interferogram, and the third-order BD will induce sidelobe [5]. The signal energy will be concentrated via dispersion compensation with a suitable trial dispersion value. The red line in the Fig. 2(b) is the BD-removed counterpart corresponding to the blue line. The labeled peak *P*1 is generated by the splicing point between the 0° polarizer and the PMF under test. While the labeled peak *P*2 denotes the polarization extinction ratio of the polarizer. Obviously, the signal energy concentration (SEC) of the interferogram without BD is the maximum.

The criterion function we use to evaluate the SEC can be expressed as

$$S(\Delta\beta_{\text{non}}) = \int I^{2m}(x)\mathrm{d}x,\ m = 2, 3, \cdots \tag{3}$$

When the power exponent equals two, the above integral formula is the signal energy of the interferogram. Next, we will verify that when there is no BD, i.e. $\Delta\beta_{\text{non}} = 0$, the criterion function exactly right takes its maximum value. Taking partial derivative of the criterion function, S, with respect to the non-linear term of propagation constant difference, $\Delta\beta_{\text{non}}(\sigma)$, we obtain

$$\frac{\partial S}{\partial \Delta\beta_{\text{non}}} = (2m-1)\int \left[I_0^{2m-1}(x) \times \frac{\partial I_0}{\partial \Delta\beta_{\text{non}}} \right] \mathrm{d}x. \tag{4}$$

Our purpose is to prove that Eq. (4) equals zero when $\Delta\beta_{\text{non}} = 0$.

Using (1), we obtain,

$$\frac{\partial H_0}{\partial \Delta\beta_{\text{non}}} = -\mathrm{i}\int_0^L [\mathrm{i}\Gamma_1(\eta)] \int_0^{+\infty} G(\sigma) e^{\mathrm{j}[2\pi\sigma x + \Delta\beta(\sigma)(L-\eta)]} \mathrm{d}\sigma \mathrm{d}\eta \tag{5}$$

where $\Gamma_1(\eta) = (L-\eta)\Gamma_0(\eta)$ is the MCC of a virtual PMF. The interferogram of it could be denoted as I_1, and the corresponding complex representation is $H_1(x)$. Then, the relationship between these two complex representations is $\partial H_0/\partial\Delta\beta_{\text{non}} = \mathrm{i}H_1$, which implies that, $\partial H_0/\partial\Delta\beta_{\text{non}} = -\mathrm{Im}[H_1]$. Since I_1 is the real part of its complex representation, we represent the foregoing partial derivative by $\partial H_0/\partial\Delta\beta_{\text{non}} = -\mathcal{H}[I_1]$, where $\mathcal{H}[I_1]$ is the conjugate function of I_1, and they could be taken Hilbert transform of each other. From (1) and (2), we know that the only difference between $I(x)$ and $I_0(x)$ is the nonlinear term of the propagation constant difference, $\Delta\beta_{\text{non}}(\sigma)$. Actually, we can regard $I_0(x)$ as a particular case of $I(x)$ when $\varphi_{\text{non,trial}}(\sigma) = 0$ in (2). Accordingly, we think that there is little difference between $I(x)$ and $I_0(x)$ when used in (4). Nevertheless, using $I(x)$ is probably more appropriate. On the other hand, the subscript 1 in $\Gamma_1(\eta) = (L-\eta)\Gamma_0(\eta)$ below (5) indicates the power exponent of the coefficient, $(L-\eta)^1$. In other words, $\Gamma_2(\eta)$ and $\Gamma_0(\eta)$ can be expressed as $\Gamma_2(\eta) = (L-\eta)^2\Gamma_0(\eta)$ and $\Gamma_0(\eta) = (L-\eta)^0\Gamma_0(\eta) = \Gamma_0(\eta)$, respectively. Thus, we used $I_0(x)$ with subscript 0 in (4).

Even though the MCCs of these two PMFs are different, the support sets, nonzero elements sets, of these two functions are identical. It means that when $\Gamma_0(\eta)$ equals zero, $\Gamma_1(\eta)$ also equals zero, and vice versa. For a single perturbation point, varying its magnitude will not change the phase of its interference fringes. For multiple perturbation points, it can be proved that the interference fringes of different peaks will not interfere when there is no BD, even if these peaks are very close. In other words, the phase of these interference fringes is identical. Consequently, if normalize the interference fringes of I_0, I_1 with their envelopes, we will find that they always overlap each other when there is no BD. It implies that $I_0^{2m-1}(x)$ and $\mathcal{H}[I_1]$ are orthogonal each other. Accordingly

$$\left.\frac{\partial S}{\partial \Delta\beta_{\text{non}}}\right|_{\Delta\beta_{\text{non}}=0} = 0 \tag{6}$$

i.e., the criterion function takes on its maximum value when there is no BD.

We should emphasize that the foregoing proof is respect to $\Delta\beta_{\text{non}}$. On the one hand, it is true not merely for the first two terms of $\Delta\beta_{\text{non}}$. Thus, this method is also able to measure higher-order BD of PMFs. On the other hand, this proof is rigorous only for an idealized PMF of which the propagation constant difference $\Delta\beta_{\text{non}}$ is identical at anywhere. For a practical PMF, we suppose that $\Delta\beta_{\text{non}}$ is nearly all the same in the select area, see Fig. 3(c). Moreover, in Fig. 3(d), we will discuss in detail the case that $\Delta\beta_{\text{non}}$ can not be regarded as a constant.

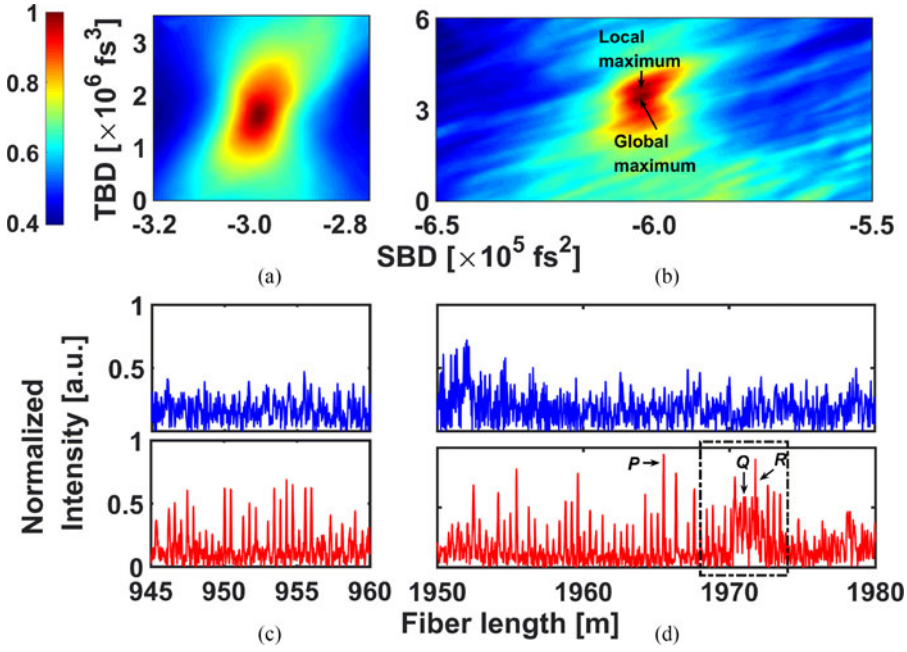

Fig. 3. Criterion function of the interferogram corresponding to the PMF in the range of (a) 945∼960 m and (b) 1950∼1980 m. Envelope of the original data and its BD-removed counterpart corresponding to the PMF in the range of (c) 945∼960 m and (d) 1950∼1980 m.

3. Results

First, we experimentally demonstrate the one-to-one correspondence between the BD of a PMF and the maximum value point of criterion function. To show the criterion function surface, we calculated every point in the select BD area with a certain step (500 × 500). However, in fact, it is unnecessary in the case of practical measurement. We chose two segments of data, in the range of 945 ∼960 m and 1950 ∼1980 m of the PMF. The criterion functions, envelopes of the interferogram (blue line), and the BD-removed counterparts (red line) are shown in Fig. 4. The interval of peaks in these comb-like counterparts is ≈0.42 m. This is due to the stress between different pieces of PMFs in adjacent circles. The dispersion compensation is implemented using the BD obtained from the corresponding criterion function in Figs. 3(a) and (b). The orderly peaks in Figs. 3(c) and (d) mean that the BD corresponding to the maximum value of criterion function is exactly the BD of these peaks.

On the one hand, the criterion function will have one global maximum value, but several local maximum values for multiple peaks with comparative intensity, see Figs. 3(b). This is because the propagation constant difference, $\Delta\beta_{\text{non}}$, varies with a large amplitude. From the perspective of signal energy, we believe that the global maximum value is matching to the BD of the peak with the largest energy. In other words, the global maximum value in Fig. 3(b) is matching to the BD of the peak *P* in Fig. 3(d). In addition, the peaks near 1971 m, such as *Q*, remains a certain BD. Therefore, we should select the appropriate range of data and provide the position of the corresponding peak when measuring the BD. On the other hand, the criterion function surface is not smooth due to the noise, then the ordinary optimization algorithm such as gradient descent is invalid. Accordingly, we employ the global optimization algorithm (GOA) to search the global maximum value of the criterion function. The specific one we use is the scatter search algorithm [15]. The calculation for the criterion function in Fig. 3(b) costs more than eight hours, whereas searching the global maximum value of it with GOA costs merely ≈1 minute by the same computer.

We have mentioned that a local maximum value is also corresponding to the BD of another peak, whereas it cannot be obtained via the GOA. Here we demonstrate how to measure it in Fig. 4. We extracted a segment of data matching to the PMF in the range of 1968 ∼1974 m from the

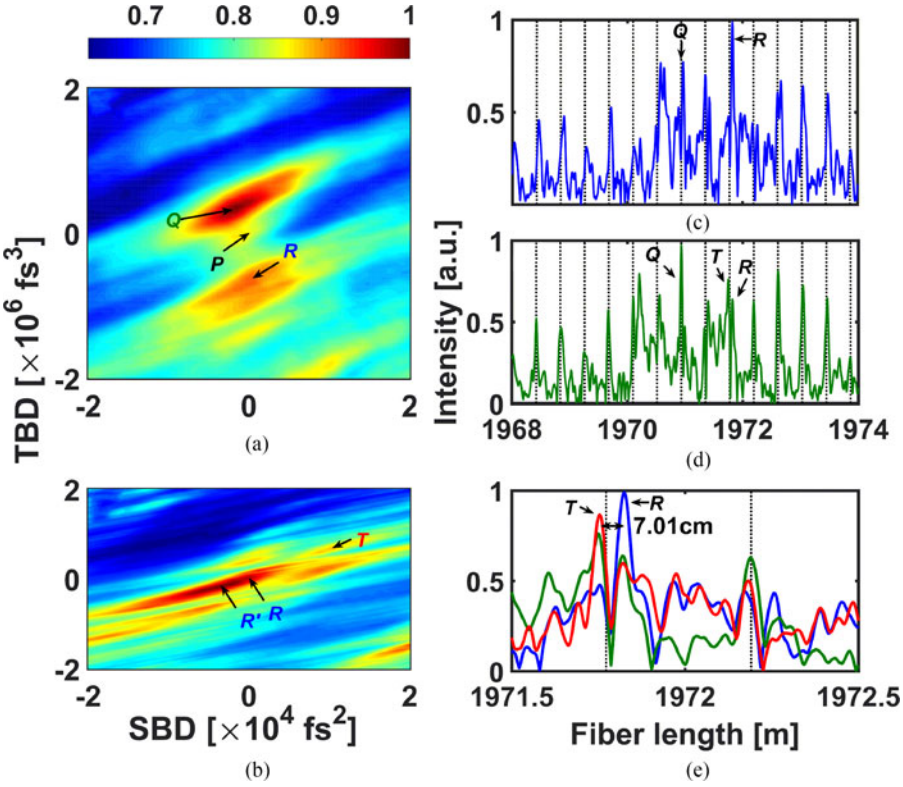

Fig. 4. Spatial resolution analysis using the data corresponding to the PMF in the range of 1968 ∼1974 m (counterpart of that in the dashed line box in Fig. 3(d)). The criterion function of this section of data after dispersion compensation with the BD of (a) peak P and (b) peak R. Envelopes of the interferogram that after dispersion compensation using the BD of (c) peak *R*, (d) peak *Q*, and (e) peak *T* (the red line). The interval of the dashed black lines is 0.42 m. The blue line and green line in Fig. 4(e) are the copies of that in Figs. 4(c) and (d). The labeled peak *Q* and *R* are the same as that in Fig. 3(d).

data that is matching to the red line in Fig. 3(d). The criterion function of the extracted data after dispersion compensation with the BD of peak *P* is shown in Figs 4(a). The labeled point *P* (0 fs^2, 0 fs^3) is corresponding to the peak *P* in Fig. 3(d). While, the points *R* (-1812 fs^2, 3.4×10^5 fs^3) and *Q* (160 fs^2, -6.72×10^5 fs^3) are corresponding to the peak *R* in Fig. 4(c) and peak *Q* in Fig. 4(d), respectively. A vector from point *P* to *Q*, $\overrightarrow{PQ}$, can denote the BD difference between peaks *P* and *Q*. Similarly, The vector $\overrightarrow{QR}$ can denote the BD difference between peaks *Q* and *R*. We can see that the two vectors have opposite directions. The interesting result is possibly because of the couple of stress between these two pieces of PMF.

To enhance the spatial resolution further, we should continue to reduce the scope of data. We chose the data corresponding to the PMF in the range of 1971.5∼1972.5 m. The criterion function of this section of data that after dispersion compensation with the BD of peak *R*. We obtained a global maximum point, *R'* (-3520 fs^2, -1.76×10^5 fs^3), near the original point. It slightly amends the BD of peak *R* obtained from Fig. 4(a). More importantly, the labeled point *T* (1.056×10^4 fs^2, 6.88×10^5 fs^3) reveals the peak *T* near the peak *R*. Accordingly, we could obtain the BD for both of these peaks, *T* and *R*. The interval of these two peaks is 7.01 cm, which implies the spatial resolution of this method is $<$10 cm. The spatial resolution for BD measurement depends on the central wavelength of the source, full width at half maximum of the source spectrum, and the birefringence of the polarization maintaining fiber under test. Besides, the spatial resolution of BD measurement should be identical to the white light interferometry.

Next the 3051 m-length PMF was tested 10 times independently, and then the 10 sets of data were processed by this method. The measurement results, 530 points in total, with error bars for

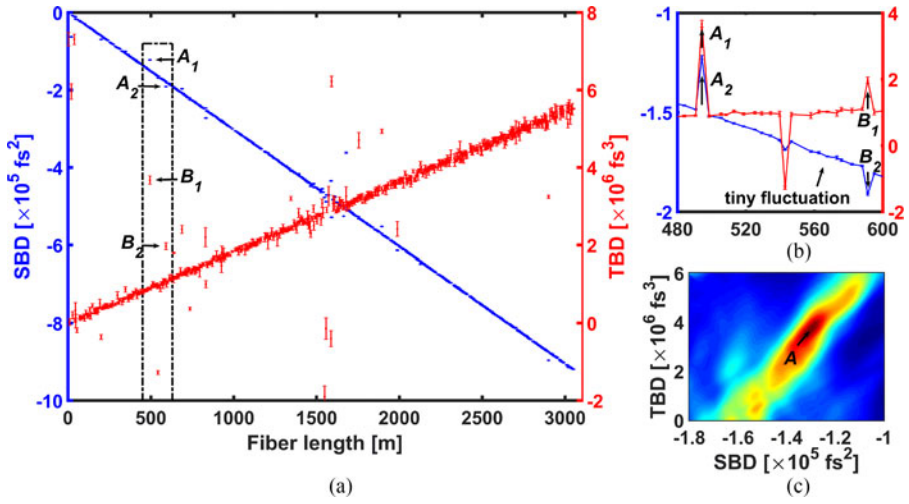

Fig. 5. (a) Distributed measurement results for second-order BD and third-order BD of the PMF. (b) Close-up of the results for PMF in the range of 480∼600 m. (c) Criterion function of the data that is corresponding to the outliers *A*1 and *A*2.

second-order BD and third-order BD of the PMF under test are depicted in Fig. 5. The average 2nd order BD and 3rd order BD of the PMF per meter can be calculated as -301.4 fs^2/m ($R^2 = 1.0000$) and 1.81×10^3 fs^3/m ($R^2 = 0.9984$), respectively, by linear fitting. Moreover, the measurement errors of 2nd order BD and 3rd order BD for all points are less than 2×10^3 fs^2 and 3×10^5 fs^3, respectively. Because the BD with respect to wavelength and its slope can be expressed as $BD(\lambda_0) = -2\pi c \cdot SBD/\lambda_0^2$, and $S(\lambda_0) = (2\pi c)^2 \cdot TBD/\lambda_0^4 + 2(2\pi c) \cdot SBD/\lambda_0^3$, the measurement repeatability for BD and its slope at 1550 nm are less than 5×10^{-4} ps/nm/km, and 2×10^{-4} ps/nm^2/km, respectively. Although the accuracy of the trial dispersion could be regarded as the same with the machine precision of the computer, the final measurement accuracy is affected by different kind of noise.

Most of the outliers in Fig. 5(a), such as *A*1, *A*2, *B*1, *B*2, are in the areas with large crosstalk, see Fig. 2(b). Thus, we believe that the remarkable fluctuation of BD is caused by the stress between PMFs on distinct circles. In addition, we can see from Fig. 5(b) that the extent and direction of deviation for points *A*1, *A*2, and *B*1, *B*2 are unlike, which perhaps due to the different stress and its direction. To verify the correctness of the outliers except for the means of error bars, we calculated the criterion function of the data in the range of 490∼498 m, which is matching to the outliers, *A*1 and *A*2. Fig. 5(c) illustrates that the measurement results in Fig. 5(b) for outliers *A*1 and *A*2 are indeed matching to the maximum value point of the criterion function. We can see tiny fluctuation of BD in Fig. 5(b) as well. Neither the remarkable nor the tiny fluctuations could be measured with those methods that can merely cope with a single perturbation point. In other words, this method is more suitable for the practical situation that is without splicing point or single stress point.

4. Conclusion

In this paper, we present a closed-loop dispersion measurement method using the signal energy concentration as feedback. Benefit from the close-loop measurement framework, dispersion measurement could be implemented in the case of low SNR. In addition, this method can cope with the multiple peaks' cases. This amounts to saying that this method could be used for distributed, not quasi-distributed, measurement. The feasibility for multiple peaks is certified with two segments of data cut from the interferogram of a 3051 m-length PMF coil. The spatial resolution of this method is identical to the TD-WLI. The distributed BD measurement for the entire PMF coil demonstrates the satisfactory performance of this method.

References

[1] J. Noda, K. Okamoto, and Y. Sasaki, "Polarization-maintaining fibers and their applications," *J. Lightw. Technol.*, vol. 4, no. 8, pp. 1071–1089, Aug. 1986.

[2] Y. Dong *et al.*, "High-sensitivity distributed transverse load sensor with an elliptical-core fiber based on Brillouin dynamic gratings," *Opt. Lett.*, vol. 40, no. 21, pp. 5003–5006, 2015.

[3] K. Okamoto and T. Hosaka, "Polarization-dependent chromatic dispersion in birefringent optical fibers," *Opt. Lett.*, vol. 12, no. 4, pp. 290–292, 1987.

[4] P. Hlubina and D. Ciprian, "Absolute phase birefringence dispersion in polarization-maintaining fiber or birefringent crystal retrieved from a channeled spectrum," *Opt. Lett.*, vol. 35, no. 10, pp. 1566–1568, 2010.

[5] T. Xu, W. Jing, H. Zhang, K. Liu, D. Jia, and Y. Zhang, "Influence of birefringence dispersion on a distributed stress sensor using birefringent optical fiber," *Opt. Fiber Technol.*, vol. 15, no. 1, pp. 83–89, 2009.

[6] P. L. Francois, F. Alard, and M. Monerie, "Chromatic dispersion measurement from Fourier transform of white-light interference patterns," *Electron. Lett.*, vol. 23, no. 7, pp. 357–358, 1987.

[7] J. Y. Lee and D. Y. Kim, "Versatile chromatic dispersion measurement of a single mode fiber using spectral white light interferometry," *Opt. Exp.,* vol. 14, no. 24, pp. 11608–11615, 2006.

[8] P. A. Merritt, R. P. Tatam, and D. A. Jackson, "Interferometric chromatic dispersion measurements on short lengths of monomode optical fiber," *J. Lightw. Technol.*, vol. 7, no. 4, pp. 703–716, Apr. 1989.

[9] D. A. Flavin, R. McBride, and J. D. C. Jones, "Dispersion of birefringence and differential group delay in polarization-maintaining fiber," *Opt. Lett.*, vol. 27, no. 12, pp. 1010–1012, 2002.

[10] P. Hlubina, T. Martynkien, and W. Urbaczyk, "Dispersion of group and phase modal birefringence in elliptical-core fiber measured by white-light spectral interferometry," *Opt. Exp.,* vol. 11, no. 22, pp. 2793–2798, 2003.

[11] F. Tang, X. Z. Wang, Y. Zhang, and W. Jing, "Distributed measurement of birefringence dispersion in polarization-maintaining fibers," *Opt. Lett.*, vol. 31, no. 23, pp. 3411–3413, 2006.

[12] H. G. Choi *et al.*, "Dispersion and birefringence of irregularly microstructured fiber with an elliptic core," *Appl. Opt.*, vol. 46, no. 35, pp. 8493–8498, 2007.

[13] Z. Yu *et al.*, "Quasi-distributed birefringence dispersion measurement for polarization maintain device with high accuracy based on white light interferometry," *Opt. Exp.,* vol. 24, no. 2, pp. 1587–1597, 2016.

[14] K. Takada and S. Mitachi, "Polarization crosstalk dependence on length in silica-based waveguides measured by using optical low coherence interference," *J. Lightw. Technol.*, vol. 16, no. 8, pp. 1413–1422, Aug. 1998.

[15] M. Laguna and R. Marti, *Scatter Search: Methodology and Implementations in C*, vol. 24. New York, NY, USA: Springer, 2012.